14TH CANADIAN MASONRY SYMPOSIUM
MONTREAL, CANADA
MAY 16TH – MAY 20TH, 2021

HOW DETAILED SHOULD YOUR MASONRY MODEL BE?

Calò, Mattia[1]; Malomo, Daniele[2]; Gabbianelli, Giammaria[3] and Pinho, Rui[4]

ABSTRACT

Recent technological advancement has enabled earthquake engineering researchers to develop numerical models of increasing complexity, capable of duly reproducing even the smallest structural detail. In the case of masonry structures, however, because of their discrete and heterogeneous nature, computational performance tends to decrease exponentially as a function of the adopted refinement level, thus confining the applicability of advanced micro-models to reduced-scale problems. For this reason, simplified modeling strategies are still largely preferred when dealing with particularly complex masonry assemblies, albeit possibly obtaining unconservative predictions especially in the case of out-of-plane-governed responses, which are typically neglected. Similarly, the effect of e.g. bond pattern, local wall-diaphragm interaction, impact phenomena and collisions are often not accounted for numerically. In current literature, however, the influence on numerical accuracy of the abovementioned simplifications has been only marginally investigated so far, while code-based modeling guidelines are missing. Thus the question posed in the title: "*how detailed should your masonry model be*?". To seek an answer, the incremental dynamic response of a shake-table-tested full-scale unreinforced masonry building specimen has been simulated in this work using a super-detailed micro-model, and the results obtained compared with those of a number of identical models in which the degree of idealization of specific elements has been purposely dwindled. Preliminary outcomes suggest that the impact of certain modeling choices are more significant than others, and that its extent significantly depends on the considered damage level.

KEYWORDS: *macro-modeling, micro-modeling, Applied Element Method, collapse analysis, shake-table test, unreinforced masonry*

[1] Ph.D. student, Department of Civil Engineering and Architecture, University of Pavia, 3 Via Adolfo Ferrata, Pavia, Italy, mattia.calo01@universitadipavia.it
[2] Assistant Professor, Department of Civil Engineering and Applied Mechanics, McGill University, 817 Sherbrooke Street, Montréal, QC, Canada, daniele.malomo@mcgill.ca
[3] Postdoctoral Fellow, Scuola Universitaria Superiore IUSS Pavia, 15 Piazza della Vittoria, Pavia, Italy, giammaria.gabbianelli@iusspavia.it
[4] Full Professor, Department of Civil Engineering and Architecture, University of Pavia, 3 Via Adolfo Ferrata, Pavia, Italy, rui.pinho@unipv.it

INTRODUCTION

In past decades, various expedite mechanism-based [1,2] and equivalent single-degree-of-freedom (SDOF) approaches were developed [3,4] for the numerical simulation of the structural response of both components e.g. [5,6] and full-scale unreinforced masonry (URM) buildings e.g. [7,8].

Previous numerical studies e.g. [9,10] also employed simplified multi-degree-of-freedom (MDOF) macroelement-based strategies, typically implemented in equivalent-frame models (EFM) based on the identification of deformable spandrel and wall components, connected through rigid node elements [11]. Despite being widely employed by practitioners and endorsed by many international codes, in presence of irregular opening layouts the identification of the effective wall height and the definition of rigid and deformable regions becomes non-unique and may lead to epistemic modelling errors [12]. Even though recent promising upgrades to this initial scheme [13,14], out-of-plane (OOP) modes often neglected, thus confining the applicability of macroelement models to in-plane (IP) governed responses [15]. The aspects above, combined with the simplified modeling of diaphragms (which e.g. neglects wall-to-diaphragm and wall-to-wall interactions), the inability to simulate responses beyond near-collapse (vital for e.g. fatality modeling), and the tendency to perform pushover analyses rather than considering dynamic loading, may result in unconservative predictions [16]. Recent technological advances have also enabled to further increase the level of complexity and detail through the use Discrete Element (DE) micro-models that have been recently employed for the seismic analysis of full-scale residential [17] and industrial [18] URM buildings made of either clay or stone units. Notwithstanding the possibility of representing explicitly fracture propagation and OOP failures, as well as both local and global collapses, the use of complex MDOF FE/DE models for the structural analysis of URM structures still requires a consistently larger amount of time, as well as very specific user skills, with respect to more simplified techniques. In current literature, however, the impact of simplified assumptions on the quality of the predicted numerical outcomes has been only marginally investigated so far, while dedicated code-based modeling guidelines are missing.

Thus the question posed in the title: "*how detailed should your masonry model be*?". To seek an answer, after having calibrated against the experimentally-observed shake-table response of a full-scale URM building specimen a reference super-detailed DE model implemented in the framework of the Applied Element Method (AEM) [19], a number of additional ones in which the degree of idealization of specific elements has been purposely decreased were created and the obtained results compared to each other.

APPLIED ELEMENT METHOD FOR MASONRY MODELING

Within the context of the AEM, masonry is typically idealized as an assembly of rigid bodies and zero-thickness nonlinear interface springs - uniformly distributed at contact surfaces - where system deformability is lumped and failure occurs, according to a micro-modeling approach. Thus, the actual texture of masonry members (see Figure 1 a)) can be explicitly reproduced numerically using the AEM, as well as damage initiation and propagation. To this end, a simplified version of

the elastic-perfectly-plastic fracture model conceived by El-Kashif and Maekawa [20] is used for representing the effect of cyclic damage due to compression loading (see Figure 1 b)). A tension cut-off criterion (with no softening branch) characterizes the spring response in tension/flexure, while shear-governed behaviors are reproduced using a Mohr-Coulomb-like model, where cohesion is set to zero right after reaching the maximum shear strength, as shown in Figure 1 c).

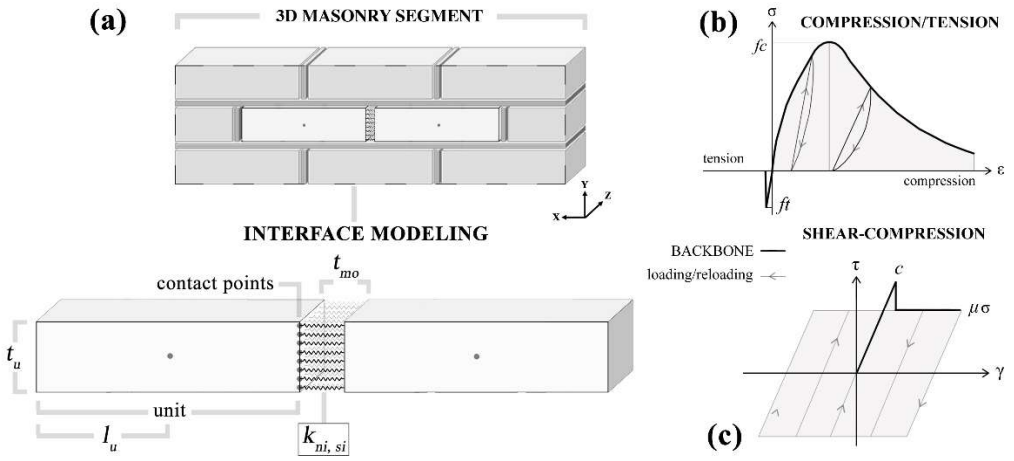

Figure 1: a) Adopted AEM discretization of a masonry cell and spring interface stiffnesses, b) compression/tension and c) shear-compression joint models

Recently, the AEM capabilities in simulating the seismic response of large-scale URM systems were investigated by various researchers, who obtained satisfactory agreement against both quasi-static [18] and dynamic [22] experimental tests on isolated URM components, as well as reduced and full-scale building specimens [23].

DETAILED MICRO-MODELING OF A FULL-SCALE URM BUILDING SPECIMEN

In this section, the construction details and main characteristics of the various sub-structures constituting the full-scale URM building specimen considered in this work, hereinafter referred to as LNEC-BUILD-3, are described and discussed together with the strategies employed to account numerically for their influence on the global dynamic response using the super-detailed (or *reference*) AEM model.

Numerical idealization of construction details

LNEC-BUILD-3 was a full-scale URM building prototype tested at the laboratory on LNEC (Lisbon, Portugal) under incremental shake-table test up to partial collapse, in the framework of a larger research project [24] aimed at assessing, amongst others, the seismic response of traditional residential URM constructions of the Groningen area (The Netherlands), which has in recenter years been subjected to low-intensity ground motions. As exhaustively discussed in [21], LNEC-BUILD-3 embodied typical features of the majority of pre-1940 detached URM houses of the Groningen building stock. Indeed, more than a proper building, it can be actually considered as an assembly of recurring structural components, including e.g. double-leaf clay brick walls (208-mm-thick) arranged according to a Dutch cross bond pattern, timber diagrams and gambrel roof, tall

chimneys, large and asymmetrical ground floor opening layout (see Figure 2). Another peculiarity of LNEC-BUILD-3 is that the thickness of the front façade is halved with respect to the other external walls, and built as a single-leaf running bond pattern URM sub-structure (100-mm-thick).

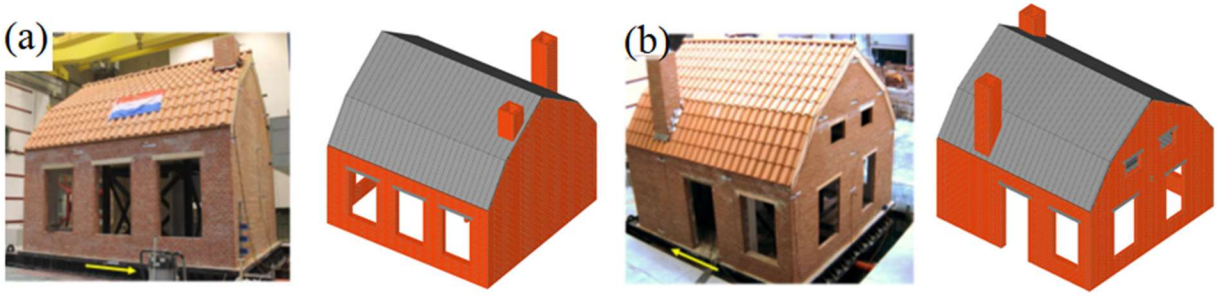

Figure 2: Photos of LNEC-BUILD-3 from a) North-West b) and South-West [21] **and related numerical model views**

The prototype building had a 2.5 m-high symmetrical gambrel roof. More precisely, the roof sub-structure combined two slopes and consisted of five timber trusses supported by fourteen purlins and a central deep ridge beam (Figure 3). The purlins extended through both gables where were pocketed into them and supported by the timber trusses. Nails were used to realize the connections between the timber elements of the roof.

Figure 3: Photos of a) roof and b) first floor of LNEC-BUILD-3 during construction [21] **and related numerical model views**

The floor consisted of timber floorboards (190-mm-wide x 24-mm-thick), nailed perpendicularly to nine pairs of timber joists (75-mm-wide x 180-mm-deep), resulting in a flexible diaphragm spanning discontinuously between the longitudinal walls (Figure 3). The floor were simply

supported at their extremities, i.e. a central timber girder (75-mm-wide x 180-mm-deep) and the external longitudinal URM walls.

Modeling of masonry elements and diaphragm sub-structures

As shown by both experimental [25] and numerical [26] investigations, the bond pattern may significantly affect the IP behavior of URM piers. For the abovementioned reason, both Dutch cross and the running bond patterns were explicitly reproduced numerically in the AEM reference model. Several mechanical characterization tests were performed prior to the shake-table test, including e.g. compression and bending tests on masonry components, bond wrench tests, direct shear-tests on triplets and torsional-shear tests on doublets. The masonry material properties selected in this paper are briefly summarized in Table 1, and include e.g. compressive strength of masonry and bricks, fc_m and fc_b respectively, flexural bond strength f_w, cohesion c and friction coefficient μ.

Table 1: LNEC-BUILD3: experimental and inferred material properties considered

	fc_m	fc_b	f_w	E_m	[1]E_b	c	μ [-]
Avg [MPa]	11.5	74.2	0.36	9120	9275	0.47	0.81
C.o.V. [%]	0.083	0.045	0.36	0.13	-	-	-

[1] derived analytically using Eurocode 6, part 1-1 [27] equations.

The abovementioned experimental material properties were not altered during the simulations, thus values presented in Table 1 were directly implemented in the AEM model.

In the framework of the experimental campaign considered in this work, previous test results indicated that the interaction among timber members and masonry elements influenced both damage propagation and gable-roof displacement capacity. Thus, in this specific case, the explicit representation of each component of the flexible diaphragms (i.e. boards, joists, purlins, etc.) was deemed necessary to attain reasonable numerical accuracy, even if it is recognized that such a detailed modelling approach is not typically employed in practical applications. Nonetheless, with a view to avoid the burdensome modelling of the actual distribution of nailed connections, as well as the employment of complex nonlinear constitutive laws for timber members (which would have increased significantly the computational expense), a meso-scale modeling strategy was undertaken that makes use of code-based and analytically-inferred mechanical parameters to be assigned to both equivalent interface springs (characterized by a rotational stiffness k_φ, in which the system nonlinearity is lumped) and linear elastic timber elements.

A bilinear constitutive law with post-peak hardening was assigned to the interface joints. Considering the initial nail shear stiffness k_0 suggested by Eurocode 5 [28], as reported in Equation 1 where ρ_m represents wood density and ϕ the nail diameter, and given the distance s_n between the nail couple, a first estimate of the initial rotational stiffness k_φ can be obtained through Equation 2 as proposed by Gattesco and Macorini [29]. Finally, the total in-plane stiffness for an unstrengthen timber floor can be obtained from Equation 3, where n_j, n_b represent the number of joists and

boards respectively and $L_{\perp,\parallel}$ is the length of the diaphragm along the load direction parallel to joists or to the boards.

$$k_0 = \left(\frac{\rho_m^{1.5} \cdot \phi^{0.8}}{30}\right) \quad (1)$$

$$k_\varphi = \left(\frac{k_0 \cdot s_n^2}{2}\right) \quad (2)$$

$$k_{\perp,\parallel} = \frac{n_j n_b k_\varphi}{L_{\perp,\parallel}^2} \quad (3)$$

The values inferred using the aforementioned parameters and implemented in the AEM models are summarized in Table 2 below:

Table 2: Load-slip parameters of nailed connections and global IP diaphragm stiffnesses

ρ_m [kg/m^3]	ϕ [mm]	s_n [mm]	k_0 [N/mm]	k_φ [kNm/rad]	$k_\parallel$ [kN/m]	$k_\perp$ [kN/m]
450	2	120	554	3.98	45.03	59.9

Shake-table results

In this sub-section, the main numerical outcomes expressed in terms of overall force-displacement hysteretic behavior at both floor and roof level are compared with the associated experimental results. It is herein recalled that LNEC-BUILD-3 was subjected to a series of unidirectional dynamic test though the consecutive application of shake-table motions of increasing intensity up to five times the reference peak table acceleration (PTA). Two different acceleration time histories were employed, i.e. SC1 (PTA=0.096g) and SC2 (PTA=0.155g). During analyses, no external dynamic relaxation schemes were introduced, meaning that the only source of damping in the proposed numerical models is the energy dissipation due to difference in loading and unloading paths of compression springs, as well as that induced by the process of crack closure/opening. Recent applications (e.g. [30]) have shown that this usually provides adequate results when considering the collapse modeling of both reduced and large-scale systems. To further scrutinize the adequacy of the reference model and quantify its capabilities in predicting the actual shake-table response of LNEC-BUILD3, ratios between numerical and experimental key quantities were computed for each test phase and summarized in Table 3. For the sake of simplicity, only values inferred considering the North-to-South shaking direction (i.e. the most relevant one, given that the recorded North-to-South - or negative – first floor displacements were 50 times larger than those measured when shaking the specimen in the opposite direction) are discussed in what follows. The factors *rBSc* and $r\vartheta^{AVG}$ define the ratio between predicted and recorded maximum base shear coefficient ($BSc = V/gm$, with is V negative base shear, g is gravitational acceleration and m is the total mass of the specimen, equal to 30.3 tons) and negative average peak floor interstory drift ϑ_{AVG} (calculated as $\Delta_x/4h$, where h=2.72 m is the height of the first floor), respectively. As confirmed by the values of the ratios (model underestimates - light blue color,

model overestimates - red color), mostly close to unity, adequate agreement was found among experimental and numerical outcomes – although the AEM model noticeably overestimated the measured displacement capacity, especially in the initial loading phases.

Table 3: Experimental vs numerical hysteretic response in terms of BSc and ϑ^{AVG}

Test ID	*BSc* Exp.	*BSc* Num.	r^{BSc} [-]	ϑ^{AVG} Exp.	ϑ^{AVG} Num.	$r\vartheta^{AVG}$ [-]
SC2-100%	-0.18	-0.18	*1.01*	-0.01	-0.02	*3.43*
SC2-150%	-0.23	-0.25	*1.06*	-0.01	-0.04	*3.55*
SC2-200%	-0.32	-0.35	*1.08*	-0.03	-0.09	*2.74*
SC2-250%	-0.43	-0.50	*1.14*	-0.25	-0.23	*0.92*
SC2-300%	-0.44	-0.60	*1.37*	-0.49	-0.41	*0.83*
SC2-350%	-0.47	-0.63	*1.32*	-0.72	-0.73	*1.02*
SC2-400%	-0.50	-0.59	*1.18*	-0.90	-1.52	*1.68*
SC2-500%	-0.59	-0.77	*1.31*	-1.90	-3.08	*1.62*

Measured vs predicted OOP response at various heights of the East gable-roof assembly is presented in Figure 4, from which it can be gathered that the reference AEM model was capable of predicting adequately the experimental displacement evolution of front façade up to the end of the test (i.e. SC2-500%). Minor differences were observed with increased damage, but it is worth noting that the signals are in phase and that relative magnitudes are comparable to each other.

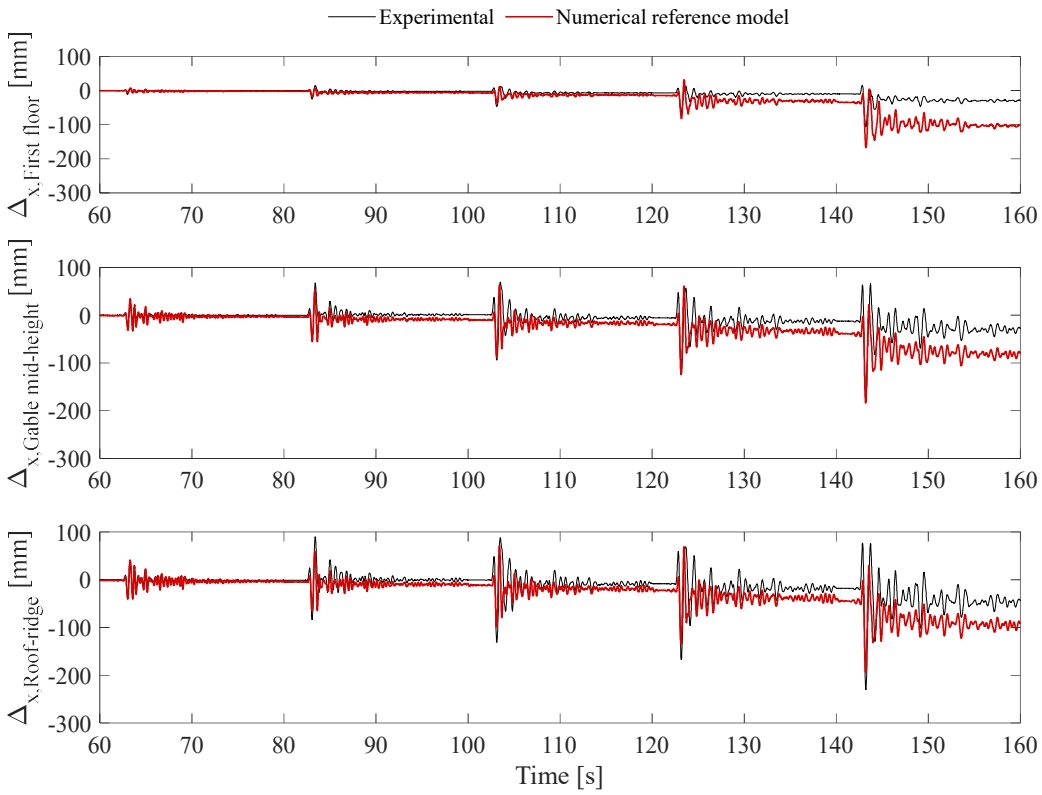

Figure 4: Experimental vs numerical displacement time-histories of gable-roof assembly

IMPACT OF MODELING REFINEMENT ON NUMERICAL RESULTS

In this section, a number of modelling scenarios are presented and discussed with the aim to scrutinize how different modelling strategies may impact numerical accuracy. Three additional models (i.e. M01, M02, M03) were considered in this sensitivity study and compared with the reference model (M0) where each structural component was explicitly model, in detail. In M01, roof system has been represented numerically as an equivalent continuous isotropic membrane which accounts for the double-slope of the LNEC-BUILD-3 gambrel roof, but neglects the explicit modeling of boards and purlins. In M02, the isotropic membrane is also used for the modeling of the first floor diaphragm, thus representing a further simplification with respect to M01. Finally, starting from the same modeling approach of M02, the influence of bond pattern on the overall response was also investigated: in M03 indeed, the Dutch-cross bond pattern is then replaced by the standard running one where each brick has been still modeled separately. The IP stiffness of the proposed membrane elements were modeled accounting for both flexural and shear deformability through the definition of an equivalent shear modulus G_d, evaluated using Equation 4, where X is shear factor, n is nail spacing, k_{ser} is the nail initial lateral stiffness, A board section and I moment of inertia of board section, while G_p and E_p stand for shear and Young's modulus parallel to grain of boards. These approaches led to a $G_{d\text{-}M01}$=5 MPa and a $G_{d\text{-}M02}$=10.7 MPa.

$$G_d = \left(\frac{X}{A}\right)\left(\frac{X}{G_p A} + \frac{L^2}{12 E_p I} + \frac{l}{k_{ser} s_n^2}\right)^{-1} \tag{4}$$

In Figure 5, the displacement time histories of the central ridge beam of the East gable-roof assembly for each of the simplified models are depicted and compared with experimental outcomes. It is worth noting that measured OOP peak displacements were significantly underestimated, especially by M03, which also exhibited an early collapse 8s after SC2-500%.

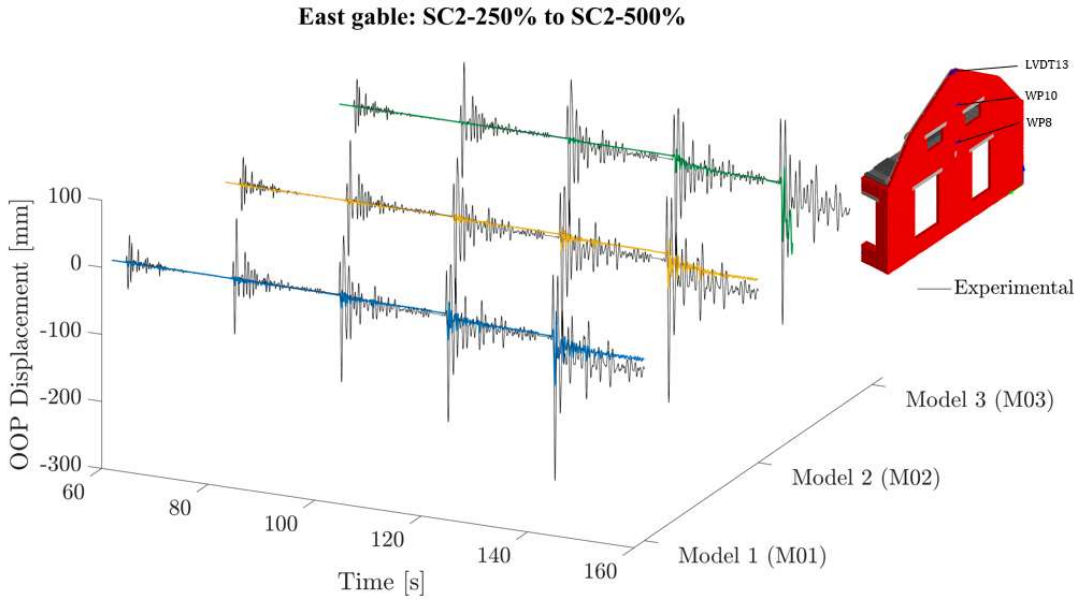

Figure 5: Exp. vs M01, M02, M03 displacement time-histories of gable-roof assembly

This might be due to the fact that the Dutch cross bond pattern here has been replaced with a standard running bond one (which tend to exhibit different failure modes, generally characterized by lower energy dissipation, see e.g. [26]), and further confirms the need to account for this aspect numerically when performing numerical analyses of URM systems.

Table 4: Experimental vs numerical (M0-03) hysteretic response in terms of BSc and ϑ^{AVG}

Test	*BSc*		*rBSc*			*ϑAVG*		*rϑAVG*		
ID	Exp.	M0	M01	M02	M03	Exp.	M0	M01	M02	M03
SC2-100%	-0.18	1.01	1.01	1.01	1.01	-0.01	3.43	3.48	2.31	1.46
SC2-150%	-0.23	1.06	1.07	1.06	0.97	-0.01	3.55	2.63	1.80	1.10
SC2-200%	-0.32	1.08	1.07	1.06	0.93	-0.03	2.74	1.56	0.95	0.59
SC2-250%	-0.43	1.14	1.07	1.09	1.07	-0.25	0.92	0.38	0.23	0.14
SC2-300%	-0.44	1.37	1.34	1.32	1.35	-0.49	0.83	0.32	0.15	0.17
SC2-350%	-0.47	1.32	1.39	1.34	1.33	-0.72	1.02	0.53	0.24	0.33
SC2-400%	-0.50	1.18	1.32	1.27	1.43	-0.90	1.68	1.14	0.69	0.97
SC2-500%	-0.59	1.31	1.49	1.53	1.47	-1.90	1.62	1.17	0.78	0.92

CONCLUSIONS

In this work, the influence of simplified modeling choices on the quality of numerical predictions of the dynamic response of an experimentally-tested URM building prototype was investigated. First, a super-detailed micro-model, M0, was developed, calibrated against test results and taken as a reference. Then, additional models M01, M02 and M03 were created based on M0 but decreasing the degree of refinement of some modeling assumptions of specific structural elements, i.e. floor and roof systems and masonry bond pattern. Despite the general good agreement in terms of hysteretic response, M0 model overestimated measured deformations and overall energy.

Significant differences among M0 and the more simplified M01-03 were observed. Overall, as expected, M0 predicted with better accuracy the experimental response in terms of base shear (Table 4, slightly overestimated though), dissipated energy and damage distribution (not included here for space constraints). With respect to the experimentally-inferred ultimate displacement capacity, M0 values were surprisingly closed to those obtained using M01 and M02. This interesting aspect might be related to the fact that the local damage due to diaphragms-to-walls dynamic interaction – overpredicted by M0, was neglected in M01-03, possibly decreasing the overall IP resistance of longitudinal façades and thus ultimate displacement capacity. In fact, this aspect could be observed in the evolution of OOP displacement of the East façade which is dramatically underestimated in all the simplified models (Figure 5). This latter response was instead significantly underpredicted by M03, whose piers indeed tended to exhibit widespread diagonal shear failures during the initial phase of the last input motion, i.e. SC2-500%, which led to the early partial collapse of the East gable.

Despite the abovementioned differences, the preliminary results presented in this work seem to suggest that a reasonable agreement might be still obtained when introducing targeted simplified

modeling assumptions – and that some may have large impact than others. Although it is not possible to formulate general rules applicable to all types of URM structural systems and loading schemes, it might be worth continuing to investigate the possibility of reducing the level of modeling detail of specific components to reduce computational time while preserving, in as much as possible, numerical accuracy.

Future research might include the evaluation of the influence of a large selection of simplified modeling strategies on e.g. seismic risk assessment studies.

ACKNOWLEDGEMENTS

The authors would like to acknowledge the reviewers for their insightful comments. In addition, the authors are grateful to all those at the Laboratório Nacional de Engenharia Civil (LNEC, Lisbon, Portugal) that were involved in the testing campaign referred to in this paper for their precious assistance in accessing the test data.

REFERENCES

[1] D'Ayala D, Speranza E. Definition of collapse mechanisms and seismic vulnerability of historic masonry buildings. Earthq Spectra 2003;19:479–509.
[2] D'Ayala D, Spence R, Oliveira C, Pomonis A. Earthquake loss estimation for Europe's historic town centres. Earthq Spectra 1997;13:773–93.
[3] Vamvatsikos D, Cornell CA. Direct estimation of the seismic demand and capacity of oscillators with multi-linear static pushovers through IDA. Earthq Eng Struct Dyn 2006;35:1097–117.
[4] Silva V, Crowley H, Pinho R, Varum H. Extending displacement-based earthquake loss assessment (DBELA) for the computation of fragility curves. Eng Struct 2013;56:343–56.
[5] Tomassetti U, Correia AA, Graziotti F, Penna A. Vulnerability of roof systems combining URM gable walls and timber diaphragms. Earthq Eng Struct Dyn 2019.
[6] Maison B, McDonald B. Fragility Curves for Residential Masonry Chimneys. Earthq Spectra 2018;34:1001–23.
[7] Borzi B, Crowley H, Pinho R. Simplified Pushover-Based Earthquake Loss Assessment (SP-BELA) Method for Masonry Buildings. Int J Archit Herit 2008;2:353–76.
[8] Snoj J, Dolšek M. Pushover-based seismic risk assessment and loss estimation of masonry buildings. Earthq Eng Struct Dyn 2020;49:567–88.
[9] Rota M, Penna A, Magenes G. A methodology for deriving analytical fragility curves for masonry buildings based on stochastic nonlinear analyses. Eng Struct 2010;32:1312–23.
[10] Pasticier L, Amadio C, Fragiacomo M. Non-linear seismic analysis and vulnerability evaluation of a masonry building by means of the SAP2000 V.10 code. Earthq Eng Struct Dyn
[11] Penna A, Lagomarsino S, Galasco A. A nonlinear macroelement model for the seismic analysis of masonry buildings. Earthq Eng Struct Dyn 2014;43:159–79.
[12] Berti M, Salvatori L, Orlando M, Spinelli P. Unreinforced masonry walls with irregular opening layouts: reliability of equivalent-frame modelling for seismic vulnerability assessment. Bull Earthq Eng 2017;15:1213–39.
[13] Malomo D, DeJong MJ. A Macro-Distinct Element Model (M-DEM) for simulating the in-plane cyclic behavior of URM structures. Eng Struct 2020;227:111428.

[14] Vanin F, Penna A, Beyer K. A three-dimensional macroelement for modelling the in-plane and out-of-plane response of masonry walls. Earthq Eng Struct Dyn 2020.
[15] Quagliarini E, Maracchini G, Clementi F. Uses and limits of the Equivalent Frame Model on existing unreinforced masonry buildings for assessing their seismic risk: A review. J Build Eng 2017;10:166–82..
[16] Silva V, Akkar S, Baker J, Bazzurro P, Castro JM, Crowley H, et al. Current Challenges and Future Trends in Analytical Fragility and Vulnerability Modeling. Earthq Spectra 2019;35:1927–52.
[17] Adhikari RK, D'Ayala D. 2015 Nepal earthquake: seismic performance and post-earthquake reconstruction of stone in mud mortar masonry buildings. Bull Earthq Eng 2020;18:3863–96.
[18] Karbassi A, Nollet M-J. Performance-based seismic vulnerability evaluation of masonry buildings using applied element method in a nonlinear dynamic-based analytical procedure. Earthq Spectra 2013;29:399–426.
[19] Meguro K, Tagel-Din H. Applied element method for structural analysis: Theory and application for linear materials. Struct Eng Eng 2000;17.
[20] El-Kashif KF, Maekawa K. Time-dependent nonlinearity of compression softening in concrete. J Adv Concr Technol 2004;2:233–47.
[21] Kallioras S, Correia AA, Graziotti F. Collapse shake - table testing of a clay - URM building with chimneys. vol. 18. Springer Netherlands; 2020.
[22] Keys RA, Clubley SK. Establishing a predictive method for blast induced masonry debris distribution using experimental and numerical methods. Eng Fail Anal 2017;82:82–91.
[23] Malomo D, Pinho R, Penna A. Simulating the shake table response of unreinforced masonry cavity wall structures tested to collapse or near-collapse conditions. Earthq Spectra 2020;36:554–78.
[24] Graziotti F, Penna A, Magenes G. A comprehensive in situ and laboratory testing programme supporting seismic risk analysis of URM buildings subjected to induced earthquakes. Bull Earthq Eng 2019;17:4575–99.
[25] Vasconcelos G, Lourenço PB. In-Plane Experimental Behavior of Stone Masonry Walls under Cyclic Loading. J Struct Eng 2009;135:1269–77.
[26] Malomo D, DeJong MJ, Penna A. Influence of Bond Pattern on the in-plane Behavior of URM Piers. Int J Archit Herit 2019.
[27] Eurocode CEN. 6: Design of masonry structures, Part 1--1: General rules for reinforced and unreinforced masonry structures. Eur Comm Stand Belgium 2005.
[28] CEN European Committee for Standardization; EN 1995-1-1:2004, Eurocode 5. Design of timber structures. Part 1–1: General rules and rules for buildings. NA to BS EN; 2004.
[29] Gattesco N, Macorini L. In-plane stiffening techniques with nail plates or CFRP strips for timber floors in historical masonry buildings. Constr Build Mater 2014;58:64–76.
[30] Calvi GM, Moratti M, O'Reilly GJ, Scattarreggia N, Monteiro R, Malomo D, et al. Once upon a Time in Italy: The Tale of the Morandi Bridge. Struct Eng Int 2019;29:198–217.